Stem Cell Reports
Article

ISSCR

OPEN ACCESS

Autism- and intellectual disability-associated *MYT1L* mutation alters human cortical interneuron differentiation, maturation, and physiology

Ramachandran Prakasam,[1] Julianna Determan,[1] Gareth Chapman,[1] Mishka Narasimhan,[1] Renata Shen,[1] Maamoon Saleh,[1] Komal Kaushik,[1] Paul Gontarz,[1] Kesavan Meganathan,[1] Bilal Hakim,[1] Bo Zhang,[1] James E. Huettner,[2] and Kristen L. Kroll[1,3,*]

[1]Department of Developmental Biology, Washington University School of Medicine, St Louis, MO 63110, USA
[2]Department of Cell Biology and Physiology, Washington University School of Medicine, St Louis, MO 63110, USA
[3]Lead contact
*Correspondence: kkroll@wustl.edu
https://doi.org/10.1016/j.stemcr.2025.102421

SUMMARY

Myelin transcription factor 1 like (MYT1L) is a neuronal transcription factor highly expressed in the developing and adult brain, and, while pathogenic *MYT1L* mutations cause neurodevelopmental disorders, these have not been characterized in human models of neurodevelopment. Here, we modeled the consequences of pathogenic *MYT1L* mutation using human stem cell-derived cortical neurons, demonstrating that *MYT1L* mutation alters the differentiation trajectory, increasing neuronal gene expression, morphological complexity, and synapse production. We also examined consequences of *MYT1L* mutation in mature cortical interneurons, identifying hallmarks of impaired neuronal identity and maturation and correspondingly altered channel expression and electrophysiological properties. Finally, by defining MYT1L genome-wide occupancy in cortical interneurons, we identified direct MYT1L targets likely to mediate these phenotypes. Together, this work elucidates new MYT1L requirements for human cortical interneuron development and demonstrates how pathogenic *MYT1L* mutation perturbs this developmental program, contributing to the etiology of neurodevelopmental disorders.

INTRODUCTION

Neurodevelopmental disorders (NDDs), including autism spectrum disorder (ASD), intellectual disability (ID), and attention deficit hyperactivity disorder (ADHD), frequently co-occur in patients and are often characterized by impaired social interaction, impaired communication, and repetitive behaviors. In recent years, genetic contributors to NDDs have been extensively profiled, identifying both *de novo* and inherited mutations in several hundred genes as contributors to NDD pathology (Gaugler et al., 2014; Havdahl et al., 2021; Zhou et al., 2022). However, only a small number of these genes have been studied in human stem cell and/or animal models to ascertain how mutations in these genes contribute to NDDs (Khodosevich and Sellgren, 2023). Among these understudied NDD-associated genes is the pro-neuronal transcription factor (TF) Myelin transcription factor 1 like (MYT1L).

Pathogenic *MYT1L* variants have been associated with an NDD syndrome (*MYT1L* syndrome) primarily characterized by ID, behavioral disorders, and obesity (Blanchet et al., 2017; Windheuser et al., 2020; De Rocker et al., 2015; Mansfield et al., 2020). Pathogenic mutations have been reported throughout the gene and include nonsense, frameshift, and missense mutations and rare cases of copy-number variants involving gene deletion, all of which are associated with NDDs (Coursimault et al., 2022), while MYT1L duplication is instead associated with increased risk of schizophrenia (Lee et al., 2012). Together, these findings link loss of MYT1L function to NDD etiology.

MYT1L is a TF and member of the neural-specific myelin transcription factor 1 family of zinc-finger TFs (Manukyan et al., 2018). While multiple studies have defined a role for MYT1L in promoting neuronal differentiation (Vierbuchen et al., 2010; Mall et al., 2017; Romm et al., 2005; Kepa et al., 2017), it has not been determined how NDD-associated *MYT1L* mutations contribute to disease etiology. MYT1L expression peaks in post-mitotic neurons during late fetal development and continues throughout life (Kepa et al., 2017; Chen et al., 2021; Kim et al., 2022), further supporting a role for MYT1L in brain development.

Several studies in mouse models have recently characterized the consequences of *MYT1L* loss-of-function (LOF) mutation or deletion (Chen et al., 2021; Kim et al., 2022; Wöhr et al., 2022; Weigel et al., 2023). These studies recapitulated some common human clinical phenotypes associated with *MYT1L* syndrome, including hyperactivity, impaired social interaction, repetitive activities, anxiety, and obesity. In examining the cellular underpinnings of these phenotypes, two models exhibited precocious neuronal differentiation, disrupted neuronal maturation, and decreased synaptic gene expression (Chen et al., 2021; Weigel et al., 2023). Other heterozygous LOF models did not exhibit precocious differentiation but instead resulted in decreased expression of synapse-related genes (Kim et al., 2022) or unaltered neurogenesis (Wöhr et al.,

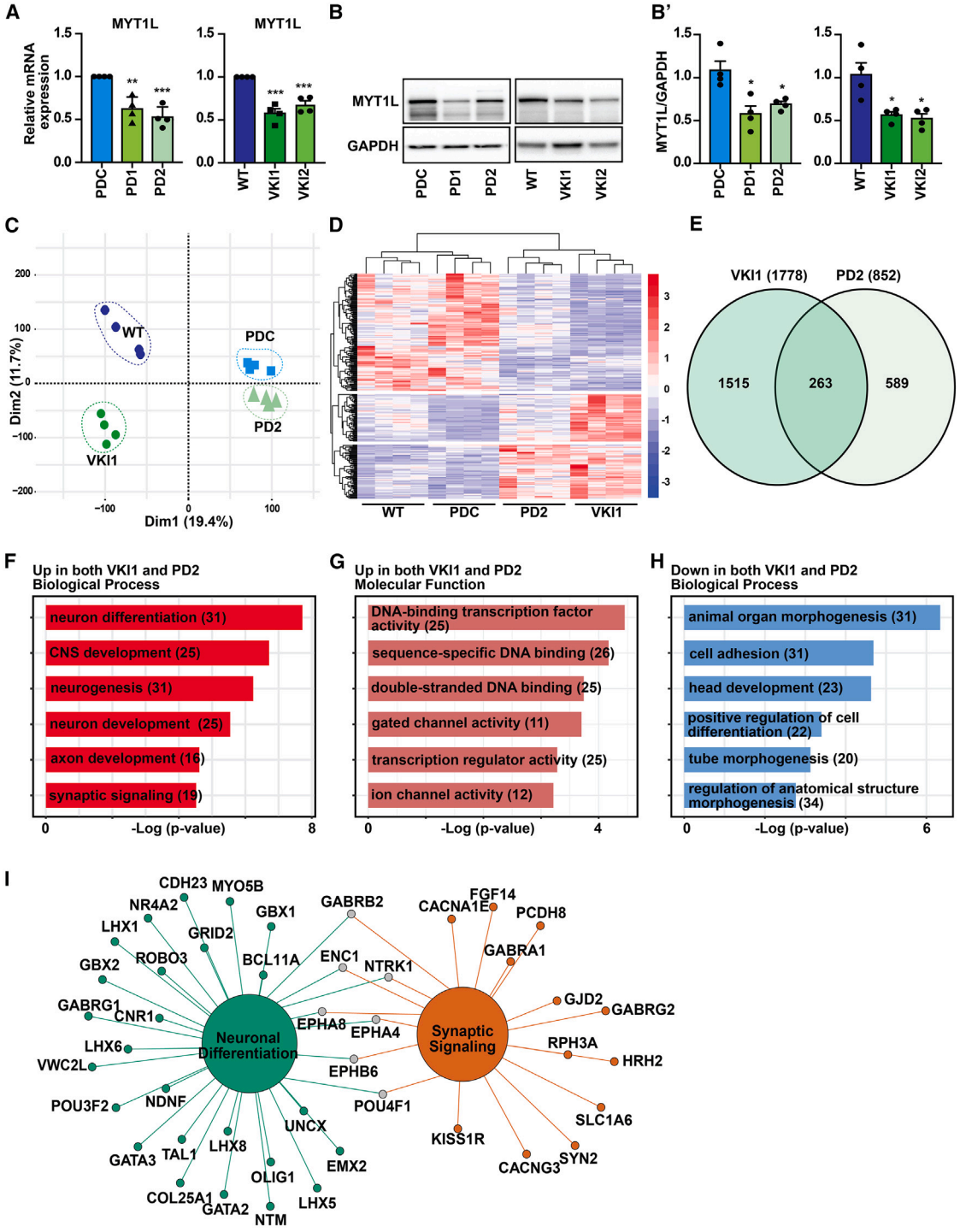

Figure 1. Transcriptomic analysis of hPSC-derived *MYT1L* S707QfsX56 variant cortical interneurons

(A) MYT1L expression was defined by RT-qPCR in cINs from the models shown.

(B) MYT1L protein levels were defined by western blotting cIN protein lysates using a MYT1L-specific antibody (GAPDH as loading control).

(B') MYT1L protein levels, normalized to loading control. All four replicates are in Figure S3D.

(C) Principal-component analysis plots visualize RNA-seq data for each model.

(D) Expression levels of differentially expressed genes (DEGs) across 4 replicates of each of cINs from these models. Red, higher and blue, lower expression.

(legend continued on next page)

2022). Given these inconsistencies, which could also relate to differences between the models and analyses performed in these studies, it remains critical to assess how pathogenic *MYT1L* mutations affect human neuronal development.

Here, we generated and characterized the first human pluripotent stem cell (hPSC) models of *MYT1L* pathogenic mutation, employing a wide range of cellular, molecular, and functional assays to understand how pathogenic *MYT1L* mutation alters neuronal development. Focusing predominantly on the development of cortical GABAergic inhibitory interneurons (cINs) as a neuronal cell type highly sensitive to NDD mutation-related perturbation (Lewis and Kroll, 2018), we defined how pathogenic *MYT1L* mutation altered cIN development. We used novel genome-wide occupancy data for MYT1L in cINs to identify MYT1L direct target genes in human cINs and correlated altered expression of these genes upon *MYT1L* mutation with cellular phenotypes related to neuronal differentiation and maturation. Ultimately, this work defined core aspects of altered neurodevelopment and function resulting from pathogenic *MYT1L* mutation, which constitute likely contributors to patient NDD phenotypes.

RESULTS

MYT1L S707Q mutation results in haploinsufficiency

We focused on an index proband subject with pathogenic *MYT1L* mutation and clinical characteristics of MYT1L syndrome, primarily developmental delay, speech delay, moderate ASD, ID, and obesity (Table S1). The subject carries a heterozygous single-nucleotide duplication in the portion of the gene encoding the MYT1L domain, converting serine 707 to glutamine and predicted to result in frameshift and a premature stop codon (S707QfsX56; Figure S1A). To characterize the consequences of this mutation, we derived hPSCs from the proband (proband derived; PD) and corrected the mutation using CRISPR genome engineering (corrected; proband derived corrected [PDC]). To examine the effect of this mutation devoid of the patient-specific genetic background, we also engineered a variant knockin model (VKI) by inserting the same mutation into wild-type (WT) hPSCs. The presence of the S707Q mutation was validated by Sanger sequencing (Figure S1B), and all models had a normal karyotype (Figure S1C), normal hPSC colony morphology, and expression of markers of pluripotency (Figure S1D).

To characterize the consequences of pathogenic *MYT1L* mutation, all models were specified as cortical interneuron neural progenitor cells (cINPCs, day [D] 15), differentiated into cINs (D30) and then further into matured cINs (m-cINs, D60), (Meganathan et al., 2017, 2023). As we observed no significant differences in cINPC specification upon *MYT1L* mutation (Figure S2), MYT1L is expressed in the developing human brain from neurogenesis *in vivo* (Figure S3A), and our previously published RNA sequencing (RNA-seq) data (Meganathan et al., 2017; Chapman et al., 2024; Sanders et al., 2022) suggest that MYT1L is largely expressed from the time of neuronal differentiation (Figure S3B), we chose to focus our studies primarily on differentiation of cINs and their maturation to m-cINs.

During the early differentiation from cINPCs to cINs (D21), we observed no change in neurosphere size between *MYT1L* variants and controls (Figures S3C and S3C′). However, relative to control models (PDC/WT), PD and VKI cINs exhibited significantly decreased MYT1L levels, as measured by mRNA (Figure 1A) and protein (Figures 1B, 1B′, and S3D). Furthermore, we did not observe a truncated protein product (predicted size 83.9 kDa), suggesting that the truncated MYT1L transcript predicted to result from S707Q mutation was eliminated by nonsense-mediated decay and thus likely reflects MYT1L haploinsufficiency.

Pathogenic *MYT1L* mutation causes upregulation of neuronal and synaptic gene expression

To investigate how the *MYT1L* S707Q LOF mutation alters gene expression, we performed RNA-seq on cINs derived from both mutant (PD, VKI) and control (PDC, WT) models. While genetic background had a significant effect across these samples with PD/PDC and VKI/WT samples clustering distinctly, the S707Q mutation produced a similar effect across both mutant versus isogenic control comparisons (Figures 1C, S4A, and S4B; Datasets S1A and S1B). Identifying differentially expressed genes (DEGs) between isogenic pairs (PD/PDC and VKI/WT), we defined 852 DEGs in the PD-PDC and 1,778 DEGs in the VKI-WT comparison (Datasets S1C and S1D). In the PD-PDC

(E) Venn diagram shows common significant DEGs for both VKI1-WT and PD2-PDC comparisons.
(F–H) Gene Ontology (GO) analysis of enriched (F) biological processes and (G) molecular functions for upregulated DEGs and enriched (H) biological processes for downregulated DEGs common to the PD2 and VKI1 models. The number of enriched genes is in parentheses.
(I) Network of upregulated DEGs under the neuronal differentiation and synaptic signaling GO terms in (F). Green nodes, neuronal differentiation; orange nodes, synaptic signaling; and gray nodes, common genes.
In all figures and panels, significance was calculated from 3 to 4 biological replicate experiments. Statistics were defined by two-tailed unpaired t test, and quantitative data are shown as mean ± SEM (methods), with $*p < 0.05$, $**p < 0.01$, and $***p < 0.001$; for all figures and panels, actual values are in Table S3.

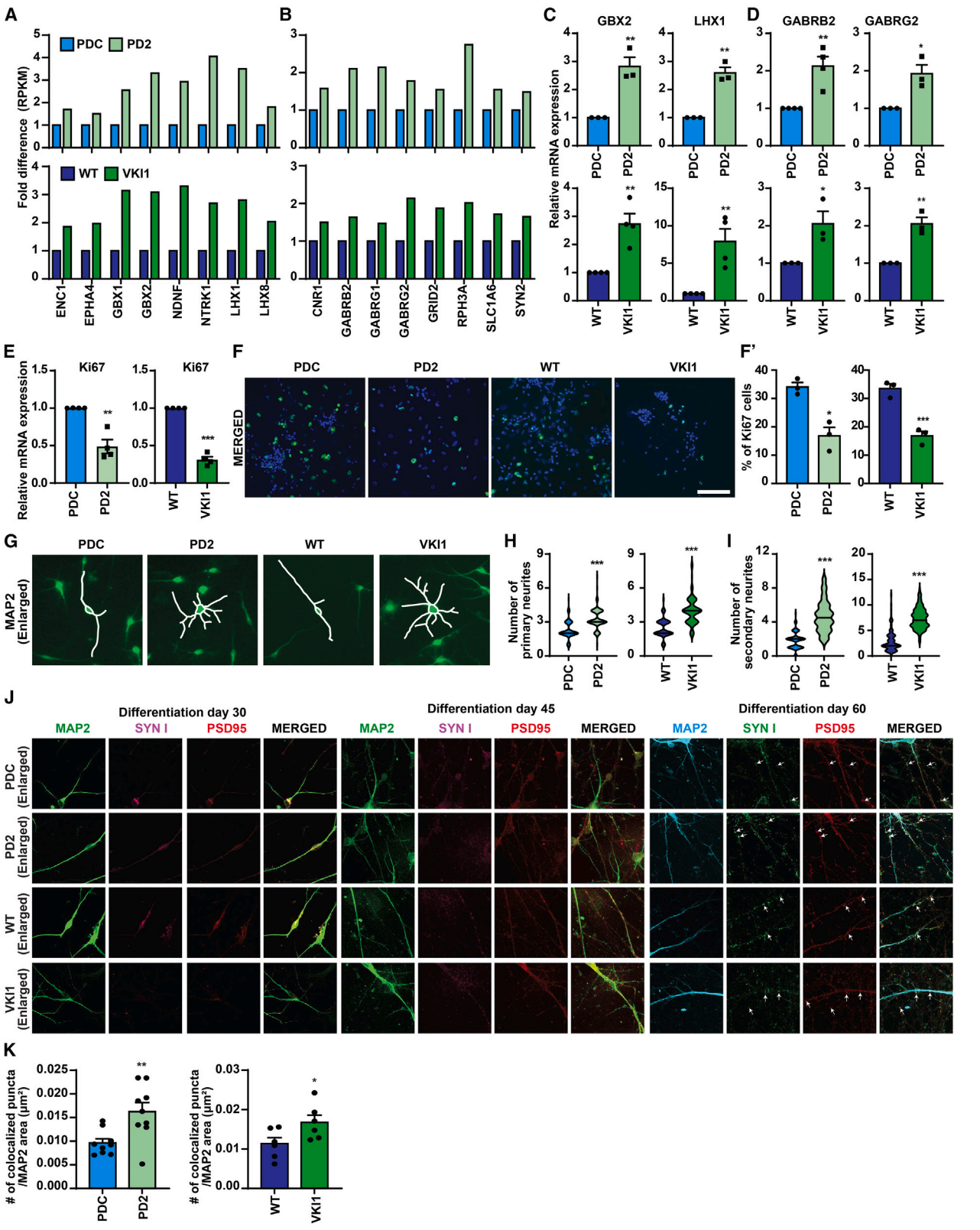

(legend on next page)

comparison, a similar number of DEGs were up- (455) versus downregulated (397) in the PD samples, while, in the VKI-WT comparison, a larger number of DEGs were downregulated (1,319) in the VKI samples (Figures S4C and S4D; Datasets S1F and S1G). Comparing the gene expression changes between models, we identified 263 common DEGs (122 up- and 141 downregulated, Figures 1D and 1E; Datasets S1E and S1H). Gene Ontology (GO) enrichment analysis of upregulated DEGs in the PD, VKI, or common datasets showed a similar enrichment for biological processes related to neuronal differentiation and synaptic signaling (Figures 1F, S4E, and S4F; Datasets S2A–S2C) and an enrichment for genes that function as TFs or as mediators of neuronal function (Figures 1G, S4E, and S4F; Datasets S2A–S2C). By contrast, downregulated DEGs across these comparisons were enriched for gene involved in early embryonic development (Figure 1H; Datasets S2D–S2F).

As many DEGs upregulated upon *MYT1L* mutation were associated with neuronal differentiation and synaptic signaling, we performed network analysis on genes associated with these GO terms, defining related gene networks (Figures 1I, S4G, and S4H). These data indicate that pathogenic *MYT1L* mutation causes upregulation of genes associated with axon development and synaptic signaling. We confirmed the upregulation of a subset of the "neuron differentiation"- and "synaptic signaling"-related genes identified by our RNA-seq analysis (Figures 2A and 2B) using quantitative reverse-transcription PCR (RT-qPCR) (Figures 2C and 2D). Together, these data demonstrate that *MYT1L* haploinsufficiency results in the upregulation of suites of neuronal gene expression.

Altered cell-cycle exit, morphology, and synaptogenesis in *MYT1L* pathogenic variant models

As the increased neuronal and synaptic gene expression we identified in the MYT1L LOF models was likely to reflect altered cIN development, we next assessed changes in cIN progenitor proliferation and cell-cycle exit accompanying differentiation. Both the PD and VKI models exhibited significantly reduced expression of the proliferative cell marker Ki67 (Figure 2E) and a ∼50% decrease in the Ki67-immuno-positive cell fraction at D30 of differentiation (Figures 2F, 2F′, S5B, and S5E). However, inclusion of DAPT in the differentiation protocol used to generate these samples raised questions as to the origin of this phenotype; therefore, we repeated these experiments either excluding DAPT or also including the CDK4/6 inhibitor PD0332997 (PD) to facilitate more efficient neuronal differentiation after Chapman et al., 2024. We confirmed a higher efficiency of cell-cycle exit in the PD and DAPT + PD differentiation protocols by examining NESTIN and Ki67 expression from D30–D60, finding a nearly complete loss of proliferating cells by D60 under those conditions (Figures S5A–S5E and S6). In these experiments, differentiation with the addition of no small molecules or DAPT only produced a similar result to that observed in our original experiments (Figures S5A and S5B); however, differentiation in the presence of PD or DAPT + PD instead yielded a very low fraction of Ki67-positive cells (∼2%) on D30, such that further reduction resulting from the *MYT1L* variant could not be assessed (Figures S5A–S5E and S6). Together, these findings indicate that *MYT1L* mutation reduces the fraction of proliferating cells, coincident with the increased expression of neuronal and synapse-related genes described earlier.

As our findings suggested that *MYT1L* S707Q mutation affected the efficiency of progenitor cell-cycle exit, we next wanted to assess if this affected neuronal morphology. Analyzing cellular morphology in cINs with bright-field imaging, we found that most control cINs exhibited bipolar morphology, while PD and VKI neurons more often exhibited a multipolar morphology (Figures S5F and S5G). Secondary neurites also increased in PD and VKI cINs (Figures S5F and S5H), with PD cell soma also being significantly larger than controls (Figure S5I). To further validate

Figure 2. *MYT1L* variant alters the neuronal differentiation and synaptic signaling gene expression and neuronal morphology

(A and B) DEGs involved in (A) neuronal differentiation and (B) synaptic signaling in the PDC-PD2 models (top) and WT-VKI1 models (bottom). Fold differences in expression of significant DEGs are represented as average reads per kilobase of transcript per million mapped reads (RPKM).

(C and D) Relative expression of the genes shown was defined by RT-qPCR in cINs.

(E) Ki67 expression, detected by RT-qPCR.

(F) Ki67 immunostained cINs (scale bar, 100 μM). (F′) percentage of Ki67-positive cells (extended images in Figure S6).

(G) Enlarged images from Figure S6J show MAP2-stained cINs, with tracing of cell soma, primary, and secondary neurites.

(H and I) (H) Primary and (I) secondary neurites were counted in cINs across 3 biological replicates and 40 cINs per replicate for each model.

(J) Enlarged images from Figure S6K of MAP2, SYN I, and PSD95 immunostained cINs. Arrows indicate SYN I, PSD95, and colocalized puncta.

(K) Quantification of colocalized SYN I/PSD95 puncta per MAP2-stained area, quantified with Imaris image analysis software.

Significance was calculated by two-tailed unpaired t test as mean ± SEM. $*p < 0.05$, $**p < 0.01$, and $***p < 0.001$.

these findings, we performed a similar quantification in MAP2 immunostained cINs, obtaining similar results (Figures 2G–2I and S5J). From these data, we concluded that *MYT1L* LOF mutation coincidently altered the efficiency of cell-cycle exit accompanying differentiation and neuronal morphology, as characterized by increased neuronal morphological complexity in the mutant lines.

Finally, to assess the effect of these changes on synapse production, we examined whether the increased morphological complexity seen earlier was accompanied by increased synapse production, as measured by the pre-synaptic marker Synapsin I (SYNI) and post-synaptic marker Post-synaptic Density Protein 95 (PSD95). Performing immunohistochemistry for these markers across three time points (D30, D45, and D60), we found these markers were significantly more abundant in m-cINs after 60 days of differentiation (Figures 2J, 2K, and S5K–S5M). Therefore, we assessed changes in the production of these markers in m-cINs in the PD and VKI models, finding an increase in SYN1 and PSD95 puncta and a concomitant increase in SYN1 and PSD95 colocalized puncta (Figures 2J, 2K, and S5K–S5M). Together, these data indicate that the *MYT1L* S707Q mutation results in more efficient progenitor cell-cycle exit, accompanied by increased morphological complexity and synapse formation.

MYT1L deficiency in the variant models impairs acquisition of neuronal and cortical interneuron identity

As we observed molecular alterations characteristic of altered cIN differentiation in the MYT1L LOF models, we next examined markers associated with neuronal and cIN identity. We found that *MYT1L* variant cINs exhibited significantly reduced expression of the pro-neuronal marker ASCL1, cIN migration marker DLX2, cIN markers calbindin 1 (CALB1), CALB2 (calretinin), and SST, and pan-GABAergic neuron markers GAD1 and GAD2 (Figures 3A–3C). We further validated these findings by immunostaining, finding that the CALB1-immuno-positive cell fraction was also significantly reduced in the variant models (Figures 3D and 3D′), which indicated that cortical interneuron and GABAergic neuron marker expression was impaired in the *MYT1L* variant model cINs. Since MYT1L was highly expressed in both cINs and cortical excitatory neurons (cExNs), we also assessed whether the mutation affected NGN2-mediated hPSC reprogramming to cExN-like neurons and found that expression of both MYT1L and the pan-neuronal markers MAP2 and β-III TUBULIN was significantly reduced in the variant models (Figures S7B and S7C), indicating that this variant similarly affected neuronal gene expression in cExNs derived by NGN2-mediated hPSC reprogramming.

MYT1L CRISPRi knockdown compromises neurite outgrowth and expression of mature neuronal and cIN markers

To establish if the phenotypes we observed were due to MYT1L LOF or were instead due to specific effects associated with the S707Q mutation, we generated two CRISPR inhibition models targeting MYT1L (gRNA G1/G2). We differentiated these models into cINs in parallel with WT control cells expressing the Cas9-KRAB fusion protein but no gRNA (KRAB) to directly assess the consequences of MYT1L knockdown (KD). Both gRNAs reduced MYT1L mRNA expression more substantially than the S707Q mutation (Figure 4A). Furthermore, unlike our PD and VKI LOF models, we observed significantly reduced neurite outgrowth from plated cINPC spheres at D20 of differentiation versus the KRAB controls (Figures 4B and 4B′). However, reminiscent of the PD and VKI LOF models, both KD models exhibited significantly reduced expression of markers of neuronal and cIN identity, including the pan-neuronal markers MAP2 and β-III TUBULIN, and of the cIN differentiation markers DLX2 and DCX, and CALB1, CALB2, SST, GAD1, and GAD2 (Figures 4C and 4D). These results were further confirmed by assessing the cell fractions immuno-positive for MYT1L, β-III TUBULIN, MAP2, and SST, which were all significantly reduced in both KD cIN models (Figures 4E and 4E′). These data indicate that MYT1L deficiency impairs the expression of general neuronal, cIN, and GABAergic neuron markers, which may compromise cIN maturation or identity.

MYT1L variant results in impaired cortical interneuron maturation

We observed reduced cIN marker expression associated with both the S707Q *MYT1L* mutation and CRISPRi-mediated KD of MYT1L in cINs, while MYT1L expression continues to increase as GABAergic neurons mature (Figures S3A and S3B). Therefore, we next assessed whether *MYT1L* deficiency also affected cIN maturation. MYT1L expression levels were reduced by 50% in m-cINs derived from PD and VKI models, relative to controls (Figure 5A). Examining the expression of pan-neuronal markers and GABAergic neuron-specific markers, we observed reduced expression of the neuronal markers MAP2 and β-III TUBULIN (Figure 5B) and similarly reduced expression of the cIN markers CALB1, CALB2, SST, GAD1, and GAD2 (Figures 5C and 5D).

To determine if these changes in gene expression were due to altered fractions of cells expressing neuronal markers, we conducted immunocytochemistry for MYT1L and MAP2 in D60 m-cINs. We found a reduction in cell proportion scored as MYT1L immuno-positive in both the PD and VKI models and a similar reduction in the proportion of MAP2-positive cells. Further analysis also showed a significant reduction of MYT1L and MAP2 double immuno-positive cells in both

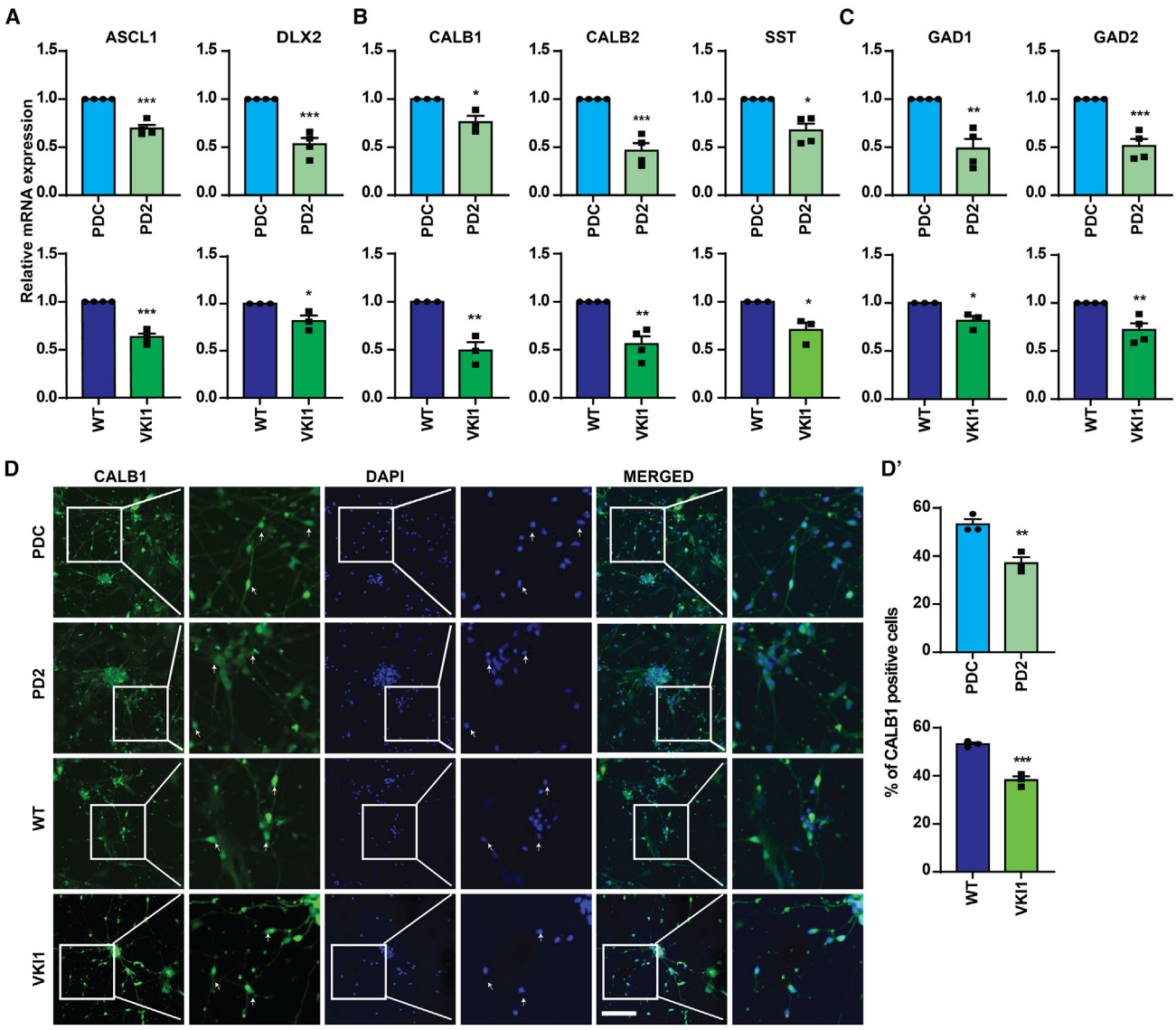

Figure 3. Expression of pro-neuronal and cortical interneuron maturation markers is diminished in cINs carrying the *MYT1L* variant

(A–C) Expression of the (A) pro-neuronal and (B and C) mature cortical interneuron markers shown, assessed by RT-qPCR in cINs.

(D) Representative images of cINs immunostained for CALB1 and DAPI counterstained. Box panels display a magnified image corresponding to the areas shown, with arrow indicating the CALB1+ and nuclei cells (scale bar, 100 μM). (D′) Percentage of CALB1-positive cells, relative to DAPI-positive nuclei.

Significance was calculated by two-tailed unpaired t test as mean ± SEM. $*p < 0.05$, $**p < 0.01$, and $***p < 0.001$.

the PD and VKI models (Figures 5E, 5E′, and S6E). Together, these data highlight that MYT1L LOF due to S707Q mutation results in a failure of GABAergic neurons to maintain expression of key neuronal and cIN markers.

Electrophysiological function and channel gene expression and activity are disrupted in *MYT1L* variant interneurons

To assess whether the MYT1L LOF mutation affected the function of GABAergic neurons, we next conducted electrophysiological recordings of VKI and WT GABAergic neurons (Figure 6). Under whole-cell voltage clamp, both the VKI and WT models could be induced to elicit an inward tetrodotoxin (TTX)-sensitive sodium (Na) current and outward 4-aminopyridine (4-AP)- and tetraethylammonium (TEA)-sensitive potassium (K) currents (Figure 6A). However, VKI GABAergic neurons exhibited significantly reduced voltage-gated currents, including diminished sodium current and both transient and sustained potassium currents (Figures 6A–6F and Table S3). In addition, VKI GABAergic

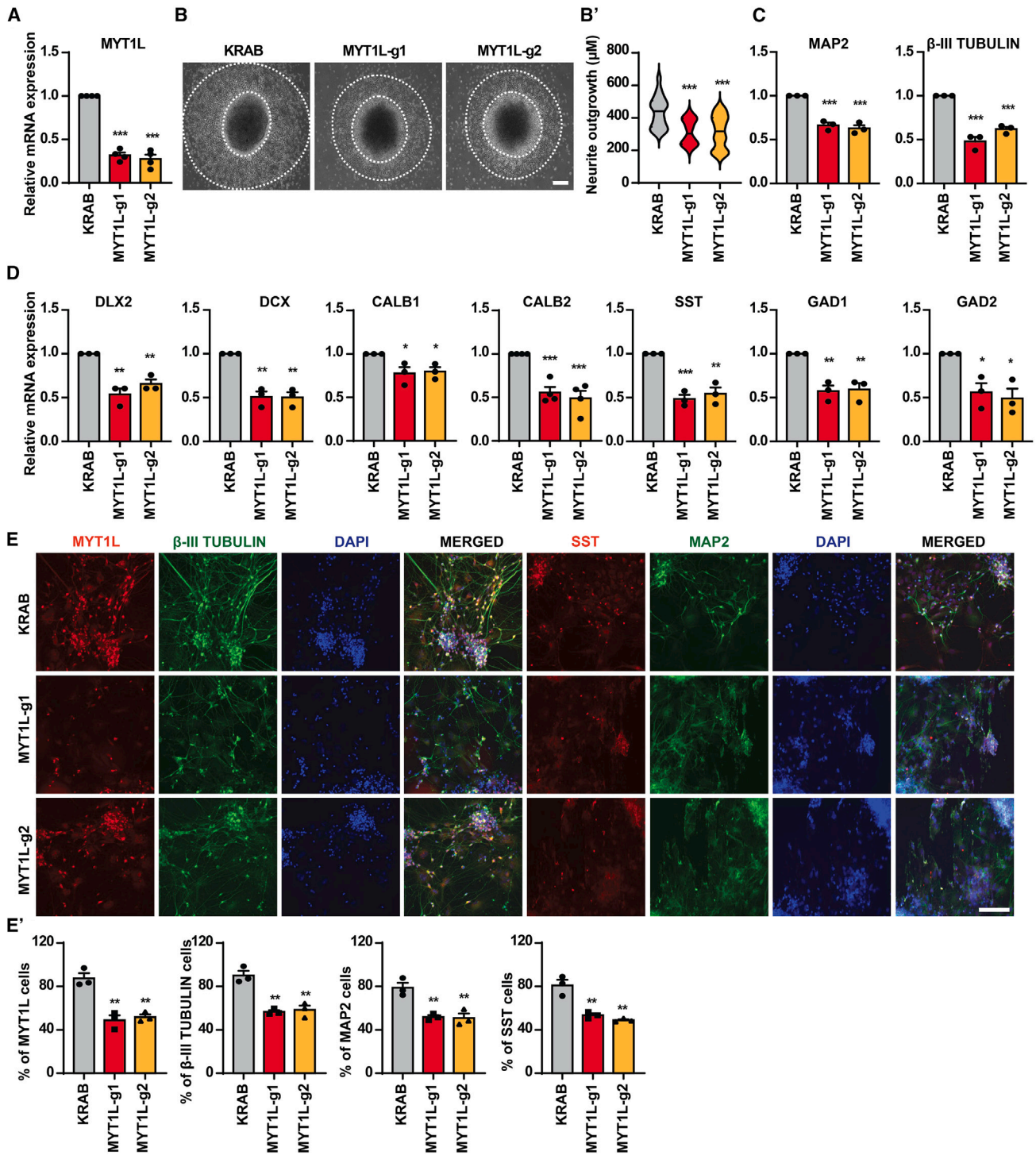

Figure 4. MYT1L knockdown compromises neurite outgrowth and neuronal differentiation and maturation marker expression

(A) MYT1L expression defined by RT-qPCR in cINs expressing dCas9-KRAB (KRAB control) +/− gRNAs.

(B) Representative images of neurite outgrowth in plated D22 spheres. Scale bar, 200 μM. Neurite outgrowth is highlighted with dotted lines. (B′) Quantification, with 14 spheres assayed per replicate.

(C and D) Expression of the markers shown, defined by RT-qPCR for the same samples.

(legend continued on next page)

neurons displayed a slightly more negative potential for steady-state current reversal (Figure 6G and Table S3). These functional changes may reflect impaired cIN identity and/or maturation and could be relevant to the etiology of neuronal circuit dysfunction associated with *MYT1L* syndrome.

To identify gene expression changes that may underlie this altered GABAergic neuron function, we examined changes in sodium and potassium ion channel expression in our cIN RNA-seq data (Dataset S2F). This analysis identified 358 genes, 39 of which were significantly downregulated in VKI cINs (Figures 6H and 6I; Datasets S1G and S2F). Therefore, reduced sodium and potassium channel expression was also associated with *MYT1L* LOF and is a potential driver of the decreased voltage-gated currents seen in electrophysiological profiling of VKI GABAergic neurons.

MYT1L binds to and regulates the promoters of neuronal genes

To determine which transcriptomic changes may be directly due to loss of transcriptional regulation by MYT1L, we used cleavage under targets and release using nuclease (CUT&RUN) to assess MYT1L genome-wide occupancy in cINs. We identified reproducible MYT1L binding sites across four biological replicate experiments (Figure 7A; Dataset S3A) and found that most sites were in gene promoters, distal intergenic regions, or introns, all sites often associated with regulatory element functions (Figure 7B). Assessing the chromatin state of MYT1L cIN binding sites using our previously published chromatin state atlas (Chapman et al., 2024), we found that MYT1L binding sites were primarily (60%) associated with active (H3K27ac and H3K4me3) marked chromatin (Figures 7C and 7D; Dataset S3B).

Performing GO enrichment analysis of the genes associated with a MYT1L binding site revealed an enrichment for other TFs, suggesting that MYT1L may act in part by controlling the expression of a suite of other TFs (Figure 7E; Dataset S3C). We also observed an enrichment for genes associated with neuronal differentiation and synapse formation (Figures 7F and 7G; Dataset S3C), suggesting that MYT1L may also affect neuronal function directly by regulating key genes involved in these processes. Integrating our MYT1L binding data with our transcriptomic data, we defined 196 PD and 558 VKI DEGs associated with a MYT1L binding site, of which 54.08% of PD and 16.8% of VKI DEGs were upregulated in the mutant cINs (Figure 7H; Dataset S4A). These were enriched for neuronal differentiation and synapse-related genes (Figures 7I and 7J; Datasets S4B–S4D), with the top 25 upregulated genes with the greatest fold change shown in heatmap view (Figure 7K; Dataset S4E). We also examined DEGs common to the PD and VKI models (Figure 1E), 63 of which were associated with MYT1L promoter-specific binding (Dataset S4F), with four examples shown as browser tracks (Figure 7L). Collectively, these data suggest that MYT1L may function to directly repress these gene classes.

Finally, to define the most likely NDD contributory MYT1L direct targets, we assessed which MYT1L-bound DEGs were high-confidence ASD (Simons Sfari; 1,076 genes; 07-20-2022 release; Dataset S4G) or epilepsy genes (EpilepsyGene; 499 genes; 05-22-2023 download; Dataset S4G), as these are common comorbidities in individuals with *MYT1L* syndrome. This analysis showed that both up- and downregulated MYT1L direct target DEGs were enriched for high-confidence ASD and/or epilepsy genes (Figures S7D and S7E, Dataset S4I), with many of these genes having known roles in neurodevelopment. These data indicate that MYT1L is required for transcriptional control of a network of downstream genes, some of which are involved in neuronal maturation and function, which likely contribute to phenotypes in individuals who carry pathogenic *MYT1L* mutation. In summary, these data indicate that *MYT1L* pathogenic mutation affects interneuron differentiation, maturation, and function (Figure S7F), effects that may relate to a requirement for MYT1L-mediated direct regulation of NDD-relevant genes, with disruption of this regulation potentially contributing to *MYT1L* syndrome-related disease pathology.

DISCUSSION

In this study, we generated the first human cellular models of pathogenic *MYT1L* mutation, using both genetic engineering and induced pluripotent stem cell paradigms and demonstrating that the *MYT1L* S707Q mutation resulted in haploinsufficiency. Differentiating these models into cortical interneurons, we found that increased neuronal and synapse-related gene expression corresponded with enhanced cell-cycle exit of progenitors and more complex neuronal morphology. As the cortical interneurons aged, we also found an associated increase in the formation of pre- and post-synaptic puncta; however, this was coupled with reduced expression of markers of mature neuronal

(E) Representative 20X images of cINs immunostained for MYT1L and β-III TUBULIN or SST and MAP2 and DAPI counterstained. Scale bar, 100 μM.

Data shown were obtained from three biological replicate experiments with significance calculated by two-tailed unpaired t test and quantitative data shown as mean ± SEM. *p* values: **p* < 0.05, ***p* < 0.01, and ****p* < 0.001.

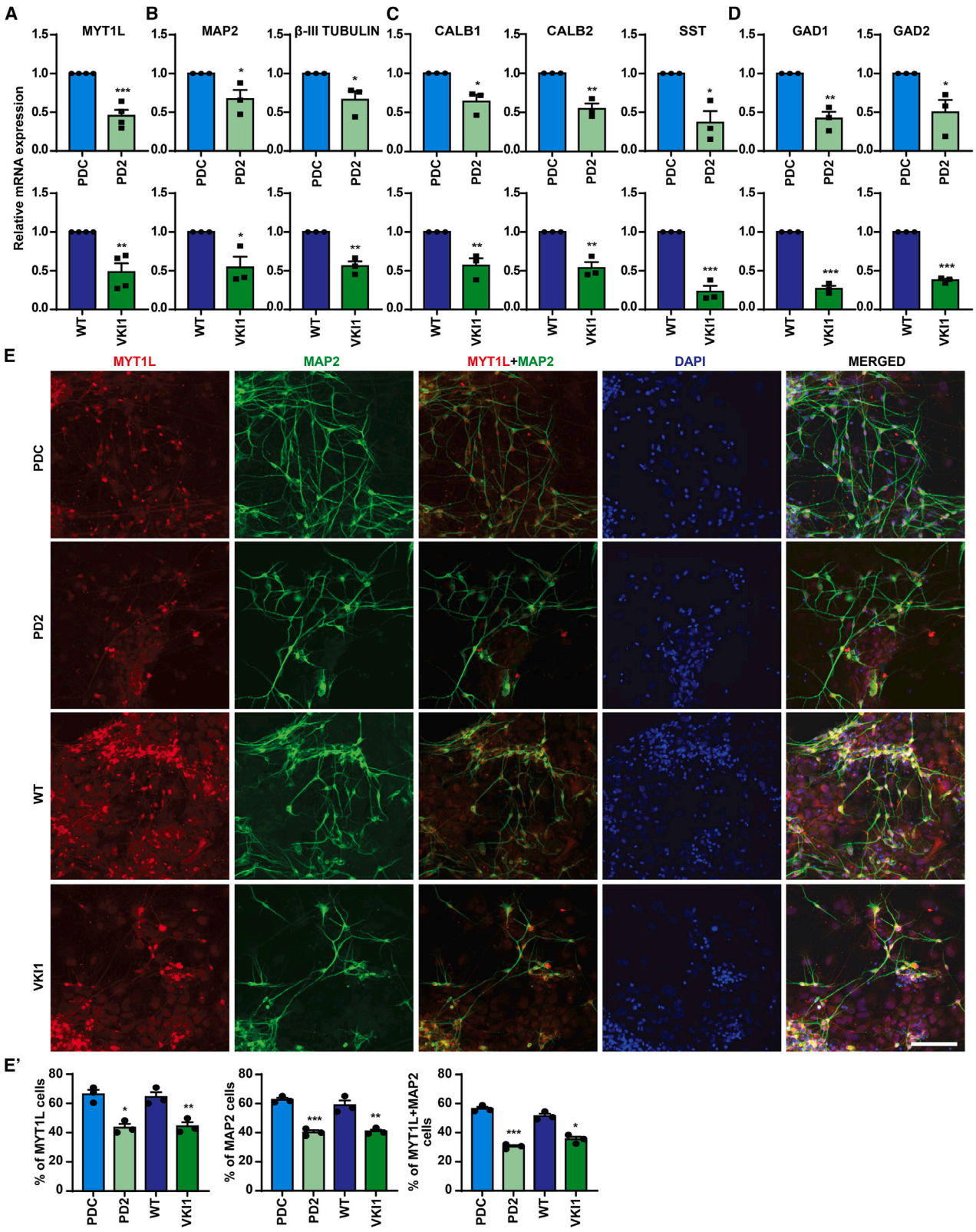

(legend on next page)

and cortical interneuron identity. Functional assessments of these *MYT1L* mutant neurons revealed reduced ion-channel currents likely caused by reductions in the expression of key channel genes. Finally, we profiled MYT1L binding in cortical interneurons and integrated these and our transcriptomic findings, highlighting a role for MYT1L in directly regulating neuronal and synaptic genes, including many NDD-related genes.

Recent work in mouse models has also focused on the analogous *MYT1L* mutation profiled in this study (c.2117dupG; MYT1L S707fsX), finding that this resulted in MYT1L haploinsufficiency and severe loss of MYT1L genome-wide binding in the developing mouse brain (Chen et al., 2021). Other recent studies have assessed Myt1l LOF in mouse models (Wöhr et al., 2022; Weigel et al., 2023; Kim et al., 2022). While differences in the analyses and time frames conducted preclude comprehensive comparisons between our human and these previously published mouse studies, both similarities and differences were observed. Distinct consequences for neurogenesis are reported in mouse models, with Chen et al., 2021 reporting that Myt1l homozygous LOF increased neuronal differentiation and expression of immature neuronal markers, while depleting stem cell and proliferative marker expressing cells in embryonic day (E)14.5 cortex (Chen et al., 2021). However, in other studies, Myt1l deficiency increased expression of the neural stem cell marker Sox2, corresponding with reduced cortical thickness and suggesting impaired neurogenesis (Weigel et al., 2023). A final study found no effects on neurogenesis associated with Myt1l LOF at E18.5 (Wöhr et al., 2022).

Beyond the effects on neurogenesis, mouse studies also found that reduction of neuron projection- and potassium ion transport-related genes was associated with loss of Myt1l function in the prefrontal cortex of adult mice (Chen et al., 2021), congruent with our findings. Likewise, heterozygous Myt1l knockout decreased striatal and hippocampal expression of synaptic genes specifically in adult mice (Kim et al., 2022), suggesting that these effects may have a later onset in murine models. Studies across Myt1l mouse models did also show some shared behavioral phenotypes at later time points including hyperactivity (Chen et al., 2021; Weigel et al., 2023). Overall, our findings here are reminiscent of the results presented by Chen et al., 2021 suggesting that loss of MYT1L expression results in increased neuronal differentiation at the expense of progenitor proliferation, followed by impaired neuronal identity and maturation.

Our results are also consistent with the known role of MYT1L in human development as a regulator of neuronal differentiation, with MYT1L expression initiated during the cell-cycle exit accompanying neuronal differentiation and peaking in the fetal and early postnatal brain (Kepa et al., 2017; www.brainspan.org). Prior work in cellular models demonstrated that Myt1l overexpression could promote neuronal conversion and maturation, while short hairpin RNA KD reduced neurite outgrowth and neuronal maturation (Vierbuchen et al., 2010; Mall et al., 2017; Kepa et al., 2017). Similarly, we found that CRISPRi-mediated MYT1L deficiency during cIN differentiation hampered neurite outgrowth and reduced the expression of pan-neuronal, cIN, and GABAergic neuron markers. By contrast, pathogenic *MYT1L* mutation had no effect on early cIN differentiation but resulted in enhanced complexity of neuronal morphology at later stages, suggesting that these phenotypes may be highly MYT1L dose dependent. However, in both the CRISPRi and mutation models, cortical interneuron marker expression was diminished, suggesting a core role for MYT1L in maintaining cIN identity. While broadly consistent with previously published studies, these results suggest a specific and more nuanced roll for MYT1L during cortical interneuron development.

While functional consequences of MYT1L mutation remain largely uncharacterized in human models, a recent study assessed altered function in cortical excitatory-like neurons generated by NGN2 overexpression-mediated reprogramming in the context of MYT1L haploinsufficiency (Weigel et al., 2023). This study reported an upregulation of synaptic gene expression, while these neurons exhibited decreased expression of neuronal-related genes and neuronal hyperactivity (Weigel et al., 2023). Therefore, our results for GABAergic neuron development are at least partially congruent with their findings for cortical glutamatergic versus neurons, although a direct comparison is challenging given the distinct models and differentiation protocols utilized. Therefore, it remains important for future studies to compare the effects of MYT1L LOF across neuronal subtypes using similar models and differentiation paradigms.

While we present the first MYT1L genome-wide binding data from human stem cell-derived cortical interneurons,

Figure 5. Expression of markers of neuronal and cortical interneuron maturation and identity is diminished in *MYT1L* variant m-cINs

(A–D) Expression of genes shown was defined by RT-qPCR in m-cINs.

(E) Representative images of m-cIN immunostained for MYT1L and MAP2 and DAPI counterstained (scale bar, 100 μM). (E′) Percentage of MYT1L, MAP2, and MYT1L + MAP2 (double)-positive cells, with significance calculated by two-tailed unpaired t test as mean ± SEM. $^{*}p < 0.05$, $^{**}p < 0.01$, and $^{***}p < 0.001$.

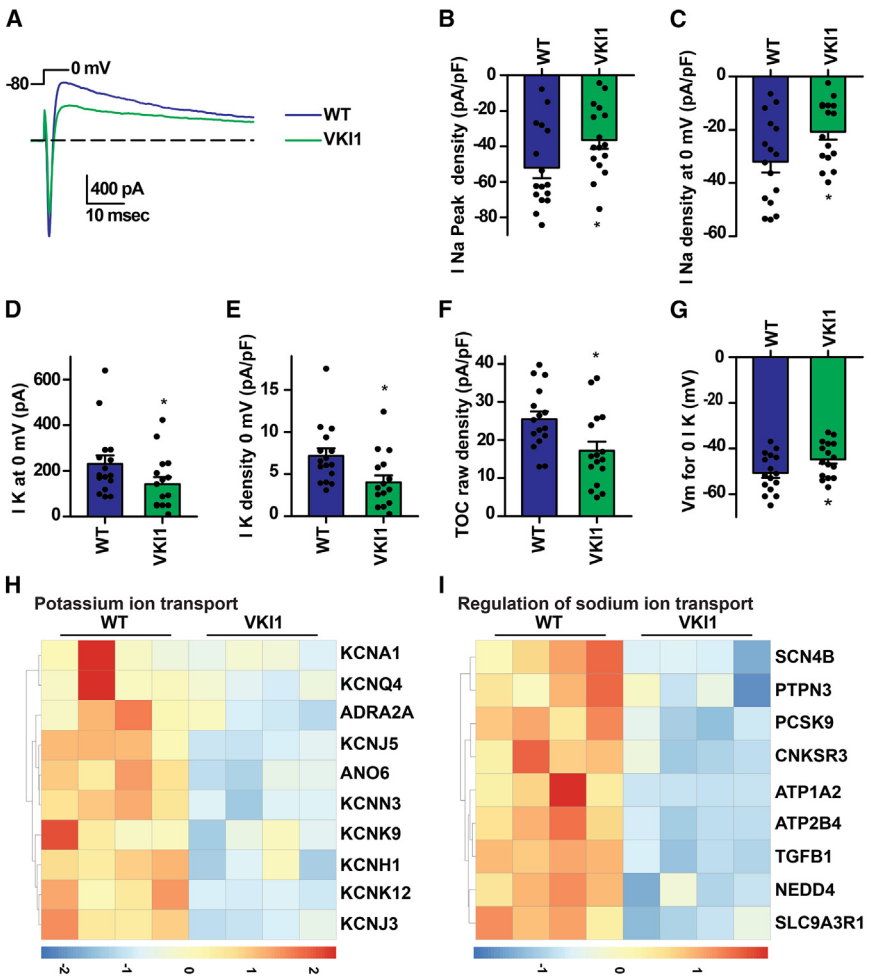

Figure 6. *MYT1L* variant m-cINs exhibit altered voltage-gated currents

(A) Inward and outward currents evoked by voltage step from −80–0 mV in neurons differentiated from WT (blue) and VKI1 (green).

(B–G) VKI1 cells had (B) reduced tetrodotoxin (TTX)-sensitive inward sodium (Na) current, (D) reduced tetraethylammonium (TEA)-sensitive steady-state outward potassium (K) current, and (C and E) reduced normalized current densities. In addition, VKI1 cells displayed (A and F) less 4-aminopyridine (4-AP; a potassium channel antagonist)-sensitive transient outward current and (G) less negative reversal potential for steady-state current.

(H and I) DEGs in VKI1-WT comparisons under the GO terms (H) potassium ion transport and (I) regulation of sodium ion transport.

Significance was calculated by two-tailed unpaired t test as mean ± SEM. $*p < 0.05$ with actual values in Table S3.

previous studies have examined MYT1L binding in mouse cortical neurons (Mall et al., 2017; Chen et al., 2023). These studies also found that Myt1l binding was predominantly associated with active histone marks found at gene promotors and putative enhancers (Mall et al., 2017; Chen et al., 2023). Consistent with our work, these studies also found that direct targets of Myt1l that were downregulated upon Myt1l LOF were enriched for NDD-associated genes, particularly those involved in synapse formation and function. Future studies may focus on these MYT1L targets as potential leads for the generation of novel interventions to treat MYT1L syndrome.

While we showed that the *MYT1L* S707Q mutation resulted in haploinsufficiency consistent with the analogous mouse model (Chen et al., 2023), it also remains to be seen whether all pathogenic *MYT1L* mutations function by haploinsufficiency. We established aspects of altered neuronal development and function that may underlie patient NDD phenotypes, including upregulation of synaptic and neuronal gene expression during differentiation, followed by impaired maturation and altered neuronal function. However, it remains critical for future studies to assess additional *MYT1L* pathogenic mutations in the paradigms utilized for this study and to compare the effects, to identify core phenotypes associated with MYT1L syndrome that may function as endophenotypes for the development of novel treatment strategies.

METHODS

Human PSC model generation

Subjects were consented for induced pluripotent stem cell (iPSC) line generation by the Washington University Institutional review board of the Human Research Protection office under human studies protocol #20163131 (Dr. Kristen L. Kroll), and all embryonic stem cell work was conducted under protocol 12-002 approved by the Washington University Embryonic Stem Cell Research Oversight (ESCRO). Proband-derived induced pluripotent

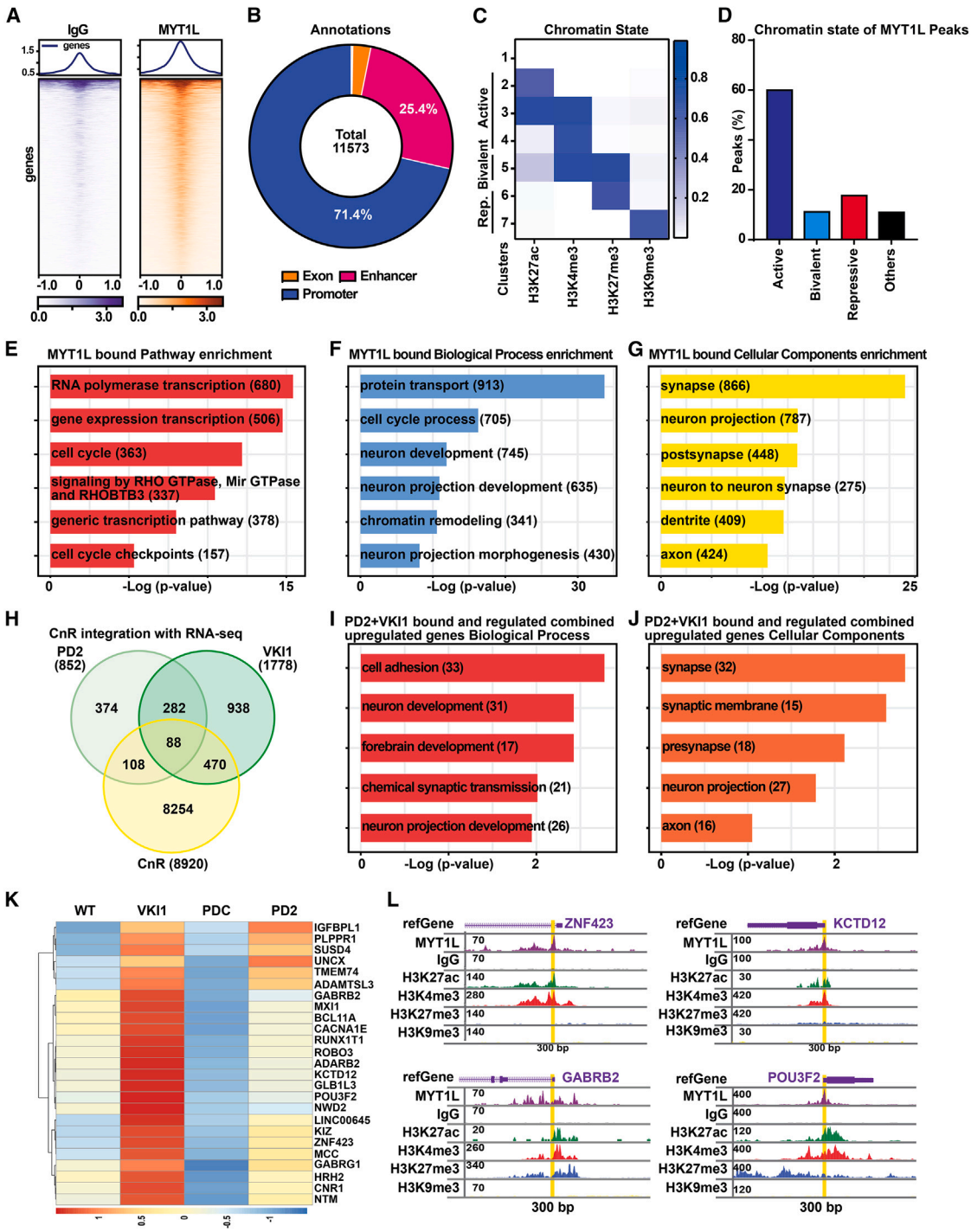

Figure 7. Genome-wide MYT1L occupancy and integration with differential gene expression in variant cortical interneurons

(A) Deep tools visualizations of MYT1L-bound peaks and immunoglobulin G (IgG) signal at the same locations ($n = 4$ [MYT1L], $n = 3$ [IgG] replicates).

(B and C) (B) MYT1L peak annotations and (C) chromatin states, defined by ChromHMM partitioning, based upon aggregate enrichment for four histone modifications from D0–D60; heatmap shows emission probabilities for the 7 clusters.

(D) MYT1L-bound peaks associated with each chromatin state.

(E–G) GO enrichment of MYT1L-bound genes.

(H) Overlap between MYT1L-bound genes and significant DEGs.

(legend continued on next page)

stem cell models (PD-iPSC) with *MYT1L* S707Q mutation and isogenic corrected iPSC lines were generated by the Washington University Genome Engineering and Stem Cell Center (GESC). Briefly, the patient's peripheral blood mononuclear cells were reprogrammed using CytoTune-iPS 2.0 Sendai reprogramming kit (Thermo Fisher Scientific), two iPSC heterozygous clones (PD1/2) were selected, PD clones were mutationally corrected to obtain isogenic PDC models, and models were Sanger sequenced to validate the mutation and correction. Lines were authenticated by STR profiling. In parallel, GESC derived hPSC models with knockin of the same variant, by genome engineering wild-type H1 (male) human embryonic stem cells (hESCs) using CRISPR-mediated genome editing.

hPSCs clonal lines were grown and maintained under feeder-free conditions in mTeSR plus medium (STEMCELL Technologies, #100-0274/75) on matrigel-coated plates at 5% CO_2 and 37°C. During standard maintenance, any hPSC colonies with morphological changes suggestive of differentiation were manually removed, hPSCs were passaged manually or using ReLeSR (STEMCELL Technologies, #100–0483), and mycoplasma testing was regularly performed (MycoAlert mycoplasma detection kit [Lonza, #LT07-118]). All lines were ensured free of bacterial and fungal contamination during stock derivation, maintenance, and experimental conditions. Clonal lines were submitted to WiCell for banking as WU-PD-MYT1L-S707Qfs (PD1 clone), WU-PDC-MYT1L-CRT (PDC), and WU-VKI_MYT1L-S707Qfs (VKI1). Cytogenetic analysis was performed by GTW banding, counting 20 metaphase cells and ensuring that all 20/20 cells for each clonal line (PDC, PD1, PD2, VKI1, and VKI2) had a normal karyotype (Figure S1C). hPSC and cINPC characterization and differentiation were done between passage numbers 1–7.

hPSC specification as cINPCs

Medial ganglionic-like neural progenitor cell (cINPC) specification was performed as previously described (Kesavan Meganathan et al., 2023). In brief, hPSC clones were dissociated with Accutase (Gibco, A11105-01) and formed into embryoid bodies (EBs) by seeded in V-bottom 96-well plates in Neurobasal complete medium (NBM: Neurobasal A 1X, Pen/Strep 1X, GlutaMAX 1X, B27 without vitamin A 1x, nonessential amino acid 1X, and 2-mercaptoethanol 1X) with small molecules (0.1 μM LDN193189 [LDN], 10 μM SB431542 [SB], 2 μM XAV939 [XAV], and 0.1 μM SAG) followed by centrifugation (200 × *g*, 5 min). EBs were maintained in NBM supplemented with LDN, SB, SAG, and XAV in V-bottom 96-well plates with feeding by $^1/_2$ media replacement every day until D4 at which point EBs were transferred to a non-adherent plasticware and incubated at 37°C and 5% CO_2 on an orbital shaker while continuing to be fed by $^1/_2$ media replacement every 2 days. On D10, EBs were plated on Matrigel- and Laminin (5 μg/mL each)-coated plasticware and were maintained in NBM supplemented with LDN, SB, SAG, and XAV until D15 at which point cells were considered cINPCs and were maintained for up to 5 passages. Passaging of cINPC was conducted using Accutase, and cells were maintained in NBM supplemented with LDN, SB, SAG, and XAV on Matrigel- and Laminin (5 μg/mL each)-coated plasticware.

cINPCs differentiation into cINs/m-cINs

For cINPC differentiation into immature cINs, cells were generated as previously described (Meganathan et al., 2017), and neurospheres were made by dissociating cINPCs with Accutase, seeding in a V-bottom plate in NBM supplemented with 10μM Y-27632 followed by centrifugation (200 × *g*, 5 min). Neurospheres were maintained in NBM with feeding by $^1/_2$ media replacement every day until D19 at which point EBs were transferred to a non-adherent plasticware and transferred to an orbital shaker. On D21, spheres were transferred to Matrigel- and Laminin-coated plasticware in NBM. Cells were fed by $^1/_2$ media changes every 2 days using NBM supplemented with DAPT (10 μM) from D22–D25, and with cyclic AMP (cAMP) (200 μM), ascorbic acid (AA: 200μM), and BDNF (20 ng) from D26–D30. Cells were considered cINs at D30 of differentiation.

m-cINs were generated using a modified protocol whereby NBM was supplemented with BDNF from D22–D26, with AA, DAPT, PD0332991 (PD, 2 μM) and BDNF from D26–D32 and AA, cAMP, and BDNF from D32–D36. On D36, NBM was replaced with BrainPhys neuronal culture medium (STEMCELL Technologies #05790) supplemented with added AA, cAMP, and BDNF. GABA (300 μM) and cytarabine (1 μM) were included from D40–D60 to promote optimal neuronal maturation and prevent unwanted glial proliferation. For experiments that tested the consequences of DAPT and/or PD treatment regimens for induction of cell-cycle withdrawal (Figures S6A–S6E), we added neither DAPT or PD, DAPT only on D22–D25, PD only on D22–D30, or PD + DAPT on D22–D30 with all samples assessed on D30.

(I and J) GO analysis of genes associated with MYT1L-bound peaks and significantly upregulated in variant cINs.
(K) Heatmap shows the average (RPKM) expression levels of the top 25 genes, with MYT1L-bound and upregulated genes shown in (H). Red, higher and blue, lower expression
(L) Browser tracks show MYT1L promoter-bound peaks, with associated histone modification state and expression levels shown in (K).

Generation of induced neurons from hPSCs

Induced neurons were generated as previously described (Schafer et al., 2019). Briefly, a construct for doxycycline-inducible overexpression of NGN2 (Addgene #127288) was stably transduced into the PDC, PD2, WT, and VKI1 hPSC models (see supplemental methods) and selected with 0.5 μg puromycin. To induce excitatory iNeurons, hPSC models were dissociated with Accutase and seeded onto Matrigel-coated plasticware in mTeSR plus media supplemented with Y-27632 and puromycin. From D0–D4, cells were fed daily with mTeSR plus containing doxycycline (DOX, 4 μg) and puromycin. On D4, media was replaced with N2B27+ (Neurobasal A [33.3%], DMEM/F-12 [66.6%], B27 supplemented with vitamin A 1X [Gibco A35828-01], N-2 supplement [Gibco 17502-048] 1X, Pen/Strep 1X, GlutaMAX 1X, nonessential amino acid 1X, and 2-mercaptoethanol 1x) supplemented with DOX and puromycin. Cultures were fed on D5 with N2B27+ supplemented with DOX, puromycin, and Cytarabine (1 μM). On D6, the cells were dissociated with Accutase and seeded on poly-D-Lysine (10 μg/mL)- and laminin (5 μg/mL)-coated plasticware. Cells continued to be fed by $^1/_2$ media change with N2B27+ supplemented with cytarabine from D6–D14 and BDNF from D8–D14. On D14, the cells were harvested, processed as described in supplemental methods.

Statistical analysis

Where appropriate, statistical analysis was carried out using a combination of GraphPad Prism version 9 (GraphPad Software; La Jolla, CA, USA, available from www.graphpad.com) and RStudio version 3.5.1 (RStudio: Integrated development environment for R; Boston, MA, USA, available from www.rstudio.org). All technical replicates were averaged before statistical analysis, and statistical tests used for each data analysis are detailed in the figure legends or in the Supplemental Methods section for specific analysis paradigms including differential gene expression analysis. A minimum of 3 independent differentiations were used for each time point or biological condition with the number of differentiations used for each sample listed in figure legends as *n*. The results in figures are presented as group mean with standard error of the mean (SEM) unless otherwise specified in figure legends. Statistical significance is indicated with asterisks as follows: ns, no significance; *, $p < 0.05$; **, $p < 0.01$; ***, and $p < 0.001$ unless otherwise specified in figure legends with all original *p* values shown in Table S3.

RESOURCE AVAILABILITY

Lead contact

Further information and requests for resources and reagents will be fulfilled by the lead contact, Kristen L. Kroll (kkroll@wustl.edu).

Materials availability

All unique/stable reagents generated in this study are available from the lead contact with a completed Materials Transfer Agreement.

Data and code availability

All raw data and processed files for RNA-seq and CUT&RUN have been deposited in NCBI/Gene Expression Omnibus database (https://www.ncbi.nlm.nih.gov/geo/) as GSE244185 and GSE244189. This paper does not report original code. Any additional information required to reanalyze these data reported is available from the lead contact upon request.

ACKNOWLEDGMENTS

We thank the GESC at Washington University School of Medicine (WUSM) for generating the iPSC and VKI models, WUSM Cytogenetics & Molecular Pathology for karyotyping services, WUCCI for the image analyses, and the WU Genome Technology Access Center at McDonnell Genome Institute (GTAC@MGI) for next-generation sequencing services. This work was supported by NIH grants R01MH124808, R01NS114551, and R01HD110556 to K.L.K.; WUSTL IDDRC P50HD103525 to J. Dougherty and C. Gurnett (K.L.K., project PI); and the Washington University Children's Discovery Institute-LI-2019-8-19, Engelhardt Family Foundation and WUSTL IDDRC Pilot Funding, and Jakob Gene Fund to K.L.K. We thank the family of the index subject for providing biomaterials for this study.

AUTHOR CONTRIBUTIONS

R.P. contributed to the study design; experiments involving D30, 45, and 60 differentiation; ICC; qPCR; western blot; CUT&RUN; CRISPRi; electrophysiology (EP); puncta quantification; data analysis; and manuscript preparation. J.D. performed D60 differentiations. M.N. and R.S. performed network analysis and visualizations. M.S. conducted morphometric assays and quantification. G.C. and K.K. generated, processed, analyzed, and visualized CUT&RUN data, and P.G. and B.Z. performed RNA sequencing data processing. K.M. performed differentiation and D30 RNA preparation. B.H. generated D30, 45, and 60 confocal images. J.E.H. conducted electrophysiology experiments, analysis, visualization, and related manuscript preparation. K.L.K. contributed to the study design, data analysis, and manuscript preparation. All authors read and approved the final manuscript.

DECLARATION OF INTERESTS

The authors declare no competing interests.

SUPPLEMENTAL INFORMATION

Supplemental information can be found online at https://doi.org/10.1016/j.stemcr.2025.102421.

Received: March 19, 2024
Revised: January 27, 2025
Accepted: January 28, 2025
Published: February 27, 2025

REFERENCES

Blanchet, P., Bebin, M., Bruet, S., Cooper, G.M., Thompson, M.L., Duban-Bedu, B., Gerard, B., Piton, A., Suckno, S., Deshpande, C., et al. (2017). MYT1L mutations cause intellectual disability and variable obesity by dysregulating gene expression and development of the neuroendocrine hypothalamus. PLoS Genet. *13*, e1006957. https://doi.org/10.1371/journal.pgen.1006957.

Chapman, G., Determan, J., Jetter, H., Kaushik, K., Prakasam, R., and Kroll, K.L. (2024). Defining cis-regulatory elements and transcription factors that control human cortical interneuron development. iScience *27*, 109967. https://doi.org/10.1016/j.isci.2024.109967.

Chen, J., Fuhler, N.A., Noguchi, K.K., and Dougherty, J.D. (2023). MYT1L is required for suppressing earlier neuronal development programs in the adult mouse brain. Genome Res. *33*, 541–556. https://doi.org/10.1101/gr.277413.122.

Chen, J., Lambo, M.E., Ge, X., Dearborn, J.T., Liu, Y., McCullough, K.B., Swift, R.G., Tabachnick, D.R., Tian, L., Noguchi, K., et al. (2021). A MYT1L syndrome mouse model recapitulates patient phenotypes and reveals altered brain development due to disrupted neuronal maturation. Neuron *109*, 3775–3792.e14. https://doi.org/10.1016/j.neuron.2021.09.009.

Coursimault, J., Guerrot, A.M., Morrow, M.M., Schramm, C., Zamora, F.M., Shanmugham, A., Liu, S., Zou, F., Bilan, F., Le Guyader, G., et al. (2022). MYT1L-associated neurodevelopmental disorder: description of 40 new cases and literature review of clinical and molecular aspects. Hum. Genet. *141*, 65–80. https://doi.org/10.1007/s00439-021-02383-z.

De Rocker, N., Vergult, S., Koolen, D., Jacobs, E., Hoischen, A., Zeesman, S., Bang, B., Béna, F., Bockaert, N., Bongers, E.M., et al. (2015). Refinement of the critical 2p25.3 deletion region: the role of MYT1L in intellectual disability and obesity. Genet. Med. *17*, 460–466. https://doi.org/10.1038/gim.2014.124.

Gaugler, T., Klei, L., Sanders, S.J., Bodea, C.A., Goldberg, A.P., Lee, A.B., Mahajan, M., Manaa, D., Pawitan, Y., Reichert, J., et al. (2014). Most genetic risk for autism resides with common variation. Nat. Genet. *46*, 881–885. https://doi.org/10.1038/ng.3039.

Havdahl, A., Niarchou, M., Starnawska, A., Uddin, M., van der Merwe, C., and Warrier, V. (2021). Genetic contributions to autism spectrum disorder. Psychol. Med. *51*, 2260–2273. https://doi.org/10.1017/S0033291721000192.

Kepa, A., Martinez Medina, L., Erk, S., Srivastava, D.P., Fernandes, A., Toro, R., Lévi, S., Ruggeri, B., Fernandes, C., Degenhardt, F., et al. (2017). Associations of the Intellectual Disability Gene MYT1L with Helix-Loop-Helix Gene Expression, Hippocampus Volume and Hippocampus Activation During Memory Retrieval. Neuropsychopharmacology *42*, 2516–2526. https://doi.org/10.1038/npp.2017.91.

Meganathan, K., Prakasam, R., Kaushik, K., Antony, I., Chapman, G., and Kroll, K.L. (2023). Derivation of Cortical Interneurons from Human Pluripotent Stem Cells to Model Neurodevelopmental Disorders (Elsevier), pp. 45–72. https://doi.org/10.1016/B978-0-12-822277-5.00007-9.

Khodosevich, K., and Sellgren, C.M. (2023). Neurodevelopmental disorders-high-resolution rethinking of disease modeling. Mol. Psychiatry *28*, 34–43. https://doi.org/10.1038/s41380-022-01876-1.

Kim, S., Oh, H., Choi, S.H., Yoo, Y.E., Noh, Y.W., Cho, Y., Im, G.H., Lee, C., Oh, Y., Yang, E., et al. (2022). Postnatal age-differential ASD-like transcriptomic, synaptic, and behavioral deficits in Myt1l-mutant mice. Cell Rep. *40*, 111398. https://doi.org/10.1016/j.celrep.2022.111398.

Lee, Y., Mattai, A., Long, R., Rapoport, J.L., Gogtay, N., and Addington, A.M. (2012). Microduplications disrupting the MYT1L gene (2p25.3) are associated with schizophrenia. Psychiatr. Genet. *22*, 206–209. https://doi.org/10.1097/YPG.0b013e328353ae3d.

Lewis, E.M., and Kroll, K.L. (2018). Development and disease in a dish: the epigenetics of neurodevelopmental disorders. Epigenomics *10*, 219–231. https://doi.org/10.2217/epi-2017-0113.

Mall, M., Kareta, M.S., Chanda, S., Ahlenius, H., Perotti, N., Zhou, B., Grieder, S.D., Ge, X., Drake, S., Euong Ang, C., et al. (2017). Myt1l safeguards neuronal identity by actively repressing many non-neuronal fates. Nature *544*, 245–249. https://doi.org/10.1038/nature21722.

Mansfield, P., Constantino, J.N., and Baldridge, D. (2020). MYT1L: A systematic review of genetic variation encompassing schizophrenia and autism. Am. J. Med. Genet. B Neuropsychiatr. Genet. *183*, 227–233. https://doi.org/10.1002/ajmg.b.32781.

Manukyan, A., Kowalczyk, I., Melhuish, T.A., Lemiesz, A., and Wotton, D. (2018). Analysis of transcriptional activity by the Myt1 and Myt1l transcription factors. J. Cell. Biochem. *119*, 4644–4655. https://doi.org/10.1002/jcb.26636.

Meganathan, K., Lewis, E.M.A., Gontarz, P., Liu, S., Stanley, E.G., Elefanty, A.G., Huettner, J.E., Zhang, B., and Kroll, K.L. (2017). Regulatory networks specifying cortical interneurons from human embryonic stem cells reveal roles for CHD2 in interneuron development. Proc. Natl. Acad. Sci. USA *114*, E11180–E11189. https://doi.org/10.1073/pnas.1712365115.

Romm, E., Nielsen, J.A., Kim, J.G., and Hudson, L.D. (2005). Myt1 family recruits histone deacetylase to regulate neural transcription. J. Neurochem. *93*, 1444–1453. https://doi.org/10.1111/j.1471-4159.2005.03131.x.

Sanders, B., D'Andrea, D., Collins, M.O., Rees, E., Steward, T.G.J., Zhu, Y., Chapman, G., Legge, S.E., Pardiñas, A.F., Harwood, A.J., et al. (2022). Transcriptional programs regulating neuronal differentiation are disrupted in DLG2 knockout human embryonic stem cells and enriched for schizophrenia and related disorders risk variants. Nat. Commun. *13*, 27. https://doi.org/10.1038/s41467-021-27601-0.

Schafer, S.T., Paquola, A.C.M., Stern, S., Gosselin, D., Ku, M., Pena, M., Kuret, T.J.M., Liyanage, M., Mansour, A.A., Jaeger, B.N., et al. (2019). Pathological priming causes developmental gene network heterochronicity in autistic subject-derived neurons. Nat Neurosci *22*, 243–255. https://doi.org/10.1038/s41593-018-0295-x.

Vierbuchen, T., Ostermeier, A., Pang, Z.P., Kokubu, Y., Südhof, T.C., and Wernig, M. (2010). Direct conversion of fibroblasts to functional neurons by defined factors. Nature *463*, 1035–1041. https://doi.org/10.1038/nature08797.

Weigel, B., Tegethoff, J.F., Grieder, S.D., Lim, B., Nagarajan, B., Liu, Y.C., Truberg, J., Papageorgiou, D., Adrian-Segarra, J.M., Schmidt, L.K., et al. (2023). MYT1L haploinsufficiency in human neurons and mice causes autism-associated phenotypes that can be reversed by genetic and pharmacologic intervention. Mol. Psychiatry *28*, 2122–2135. https://doi.org/10.1038/s41380-023-01959-7.

Windheuser, I.C., Becker, J., Cremer, K., Hundertmark, H., Yates, L.M., Mangold, E., Peters, S., Degenhardt, F., Ludwig, K.U., Zink, A.M., et al. (2020). Nine newly identified individuals refine the phenotype associated with MYT1L mutations. Am. J. Med. Genet. *182*, 1021–1031. https://doi.org/10.1002/ajmg.a.61515.

Wöhr, M., Fong, W.M., Janas, J.A., Mall, M., Thome, C., Vangipuram, M., Meng, L., Südhof, T.C., and Wernig, M. (2022). Myt1l haploinsufficiency leads to obesity and multifaceted behavioral alterations in mice. Mol. Autism *13*, 19. https://doi.org/10.1186/s13229-022-00497-3.

Zhou, X., Feliciano, P., Shu, C., Wang, T., Astrovskaya, I., Hall, J.B., Obiajulu, J.U., Wright, J.R., Murali, S.C., Xu, S.X., et al. (2022). Integrating *de novo* and inherited variants in 42,607 autism cases identifies mutations in new moderate-risk genes. Nat. Genet. *54*, 1305–1319. https://doi.org/10.1038/s41588-022-01148-2.